AIAA JOURNAL
Vol. 39, No. 3, March 2001

# Aerodynamic Flow Control over an Unconventional Airfoil Using Synthetic Jet Actuators

Michael Amitay*
*Georgia Tech Research Institute, Smyrna, Georgia 30080*
Douglas R. Smith†
*University of Wyoming, Laramie, Wyoming 82071-3295*
Valdis Kibens‡
*The Boeing Company, St. Louis, Missouri 63166*
David E. Parekh§
*Georgia Tech Research Institute, Smyrna, Georgia 30080*
and
Ari Glezer¶
*Georgia Institute of Technology, Atlanta, Georgia 30332-0405*

**Control of flow separation on an unconventional symmetric airfoil using synthetic (zero net mass flux) jet actuators is investigated in a series of wind tunnel tests. The symmetric airfoil comprises the aft portion of a NACA four-digit series airfoil and a leading edge section that is one-half of a round cylinder. The experiments are conducted over a range of Reynolds numbers between $3.1 \times 10^5$ and $7.25 \times 10^5$. In this range, the flow separates near the leading edge at angles of attack exceeding 5 deg. When synthetic jet control is applied near the leading edge, upstream of the separation point, the separated flow reattaches completely for angles of attack up to 17.5 deg and partially for higher angles of attack. The effect of the actuation frequency, actuator location, and momentum coefficient is investigated for different angles of attack. The momentum coefficient required to reattach the separated flow decreases as the actuators are placed closer to the separation point. In some cases, reattachment is also achieved when the actuators are placed downstream of the stagnation point on the pressure side of the airfoil. Control effectiveness is distinctly different for low and high actuation frequencies and is influenced by the disparity of the characteristic timescale of the actuation.**

## I. Introduction

OPTIMUM aerodynamic performance that avoids flow separation on wing surfaces has been traditionally achieved by appropriate aerodynamic design of the airfoil section. However, when the wing design is driven by nonaerodynamic constrains, stealth, for example, the lift and drag performance of the resulting unconventional airfoil shape may be severely diminished, and either active or passive flow control is necessary to maintain aerodynamic performance throughout the normal flight envelope.

The present work is part of a series of related studies[1,2] that have explored the utilization of synthetic (zero net mass flux) jet flow control for the modification of the lift and drag characteristics of bluff bodies. The current contribution focuses on improving the aerodynamic performance of unconventional airfoil shapes whose designs emphasize optimization of mission objectives at the cost of vehicle aerodynamics.

Although passive control devices, for example, vortex generators, have proven to be quite effective in delaying flow separation, under some conditions, they afford no proportional control and introduce a drag penalty when the flow does not separate. In contrast, active control approaches enable coupling of the control input to flow instabilities that are associated with flow separation and, thus, may enable substantial control authority at low actuation levels. Furthermore, active actuation is largely innocuous except when activated and has the potential for delivering variable power.

In previous studies, active control efforts have employed a variety of techniques including external and internal acoustic excitation,[3,4] vibrating ribbons or flaps,[5] and steady and unsteady blowing/bleed.[6] Various degrees of separation control were achieved by manipulating the unstable separated free shear layer leading to a complete or a partial reattachment of the separated flow. External acoustic excitation for separation control on an airfoil was investigated by Ahuja and Burrin[3] and Zaman et al.,[4] who exploited the acoustic resonance in the wind-tunnel test section to induce cross-stream velocity perturbations. Zaman et al.[4] noted that the introduction of oscillatory cross-stream velocity perturbations by other means might be more viable for excitation of separated airfoil flows.

Internal acoustic excitation for separation control was first investigated by Huang et al.[5] and Hsiao et al.,[6] who used an acoustically driven cavity within a NACA $63_3$-018 airfoil to excite the boundary layer through a small rectangular orifice placed near the leading edge of the airfoil. Both studies used the sound pressure level (SPL) above the orifice to characterize the control input. Whereas the work of Huang et al.[5] was limited to the shedding frequency of the airfoil, that is, dimensionless frequency $F^+ \sim 1$, Hsiao et al.[6] investigated a broader range of actuation frequencies up to $F^+ \sim 20$. These authors achieved a 40% increment in the lift coefficient at poststall angles of attack. In a later study on the effects of internal excitation on flow separation from a circular cylinder, Williams et al.[7] noted that the correct measure of the actuation amplitude is the unsteady velocity at the orifice rather than the SPL. In the subsequent work of Chang et al.[8] on a two-dimensional airfoil (NACA $63_3$-018), the orifice velocity was calibrated with respect to frequency, and the authors were able to demonstrate the effect of frequency on separation control at low poststall angles of attack ($15 < \alpha < 20$ deg) at $Re_c = 3 \times 10^5$. For small levels of momentum coefficient $C_\mu < 10^{-4}$ (computed based on the amplitude of the velocity oscillations), separation control correlated strongly with the frequency of the shear

Received 8 January 2000; revision received 20 September 2000; accepted for publication 22 September 2000. 

*Research Engineer, Aerospace, Transportation and Advanced Systems Laboratory. Member AIAA.
†Assistant Professor, Mechanical Engineering Department. Member AIAA.
‡Associate Technical Fellow, Phantom Works. Associate Fellow AIAA.
§Director, Aerospace, Transportation and Advanced Systems Laboratory. Associate Fellow AIAA.
¶Professor, School of Mechanical Engineering. Member AIAA.

layer instability ($F^+ \cong 2$) and resulted in up to a 50% increase in lift. However, larger levels of $C_\mu (> 10^{-4})$ led to effective control of separation over a much broader range of frequencies ($2 < F^+ < 20$). At higher poststall angles of attack ($20 < \alpha < 25$ deg) Hsiao et al.[9] reported that the actuation frequency that resulted in improved aerodynamic performance correlated with the vortex-shedding frequency in the airfoil wake.

Forcing of a separated flow by means of oscillatory net mass injection tangential to the flow surface has been found to be an effective means for control of separation with substantially less mass flux than required from steady blowing. In an investigation of steady and unsteady blowing at the hinge of a 25% chord flap on a NACA 0015 airfoil, Seifert et al.[10] showed that an oscillatory blowing ($C_\mu < 0.016$) combined with a low level of steady blowing ($C_\mu < 0.008$) proved to be the most efficient actuation method. Adding an oscillatory component at 20-deg flap deflection and small angle of attack led to lift coefficient increments of 0.5 over steady blowing. (These authors used a reduced dimensionless frequency $F^+$, which is based on the actuation frequency and the length scale of the separated flow region.) The results of Seifert et al.[10] showed that excitation at reduced frequencies $F^+$ between 1 and 3 provided the most effective flow reattachment over the flap. In a similar investigation, Seifert et al.[11] used unsteady blowing with net mass flux at a leading edge of NACA0015 airfoil. Here, the frequency scaling for correlating $C_\mu$ was found to depend on the length over which reattached flow was to be maintained. Interestingly, surface pressure measurements phase locked to the actuation frequency suggested that the flow was not reattached in a steady sense. A related numerical simulation of the flow about an NACA0012 airfoil forced by a synthetic (zero net mass flux) oscillating jet operating at $F^+ \cong 1$ (Ref. 12) demonstrated a 20% increase in lift at a poststall angle of attack of $\alpha = 22$ deg that appeared to corroborated the measurements of Seifert et al.[11] at a similar $F^+$. However, large intermittent separated flow regions (at the actuation frequency) resulted in substantial oscillations in lift (up to 20% peak-to-peak).

Several investigations have demonstrated control of flow separation over bluff bodies using synthetic (zero net mass flux) jet.[1,2] The formation and evolution of synthetic jets is described in detail in the work of Smith and Glezer.[13,14] To review briefly, these jets

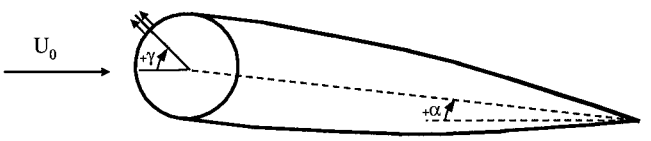


**Fig. 1 Airfoil model.**

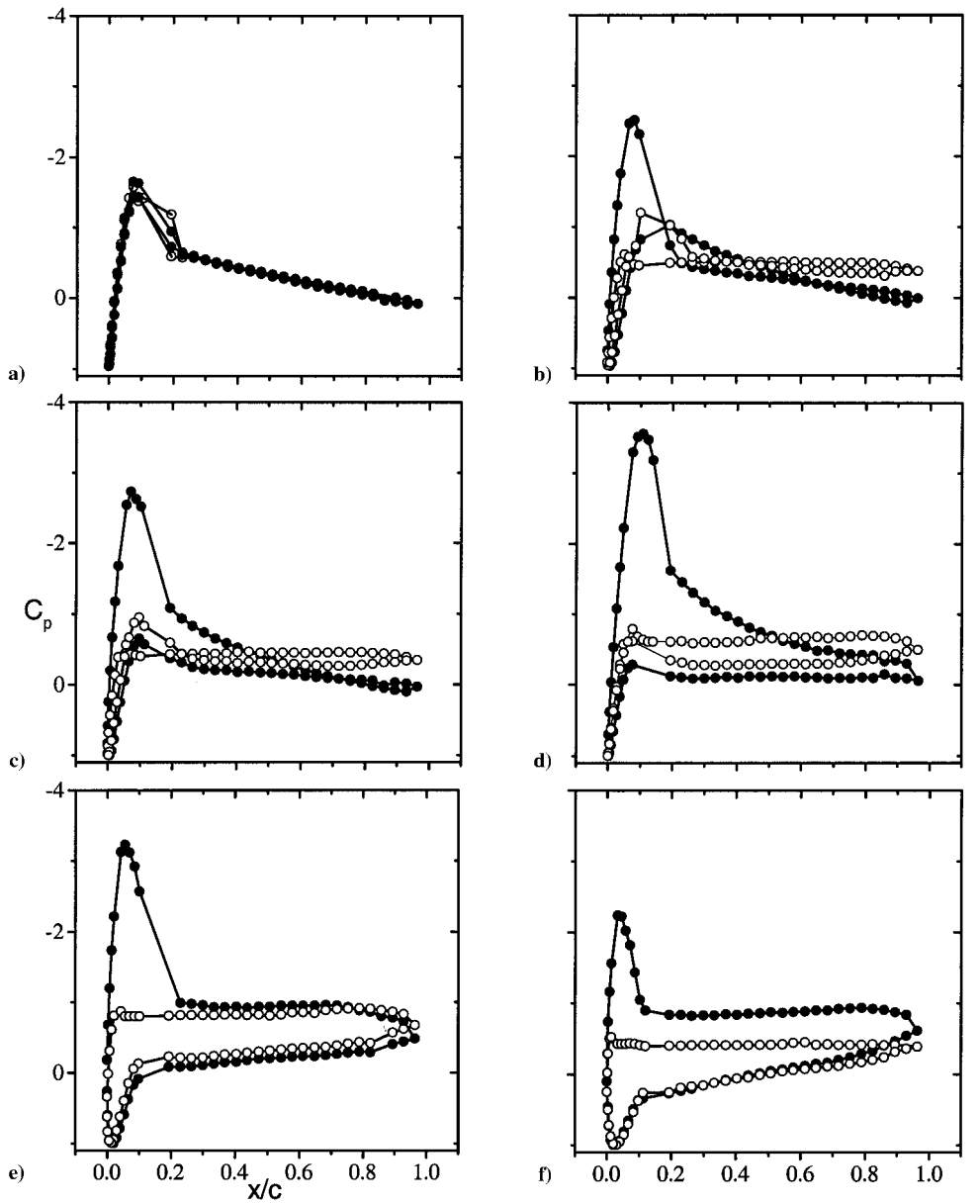


**Fig. 2 Forced (●) and unforced (○) cases; pressure coefficient distributions around the airfoil at different angles of attack: a) $\alpha = 0$ deg, b) $\alpha = 5$ deg, c) $\alpha = 10$ deg, d) $\alpha = 15$ deg, e) $\alpha = 20$ deg, and f) $\alpha = 25$ deg.**

are turbulent jets that are formed at an orifice to a small cavity by the time-periodic motion of a diaphragm on one of the cavity walls. Although synthetic jets are zero net mass flux in nature, they do impart a net linear momentum to the ambient fluid. The interaction of synthetic jets with a crossflow can lead to an apparent modification of the aerodynamic shape of bluff bodies and, thus, provides a means for control of separated shear flows. This approach was demonstrated by Amitay et al.[1,2] on a circular cylinder. Depending on the azimuthal position of the jets, a new aerodynamic profile of the cylinder was apparent as the base pressure increased and an asymmetric pressure distribution developed around the cylinder. This improved profile had up to 30% lower pressure drag coefficient and a peak steady lift coefficient of 0.9 and was achieved with a relatively low momentum coefficient $C_\mu = \mathcal{O}(10^{-4})$ at a nondimensional frequency (patterned after the Strouhal number) of 2.6. This dimensionless frequency is an order of magnitude larger than the Strouhal number associated with the natural shedding frequency of the cylinder ($Sr = 0.2$).

The current work is concerned with improvements of the aerodynamic performance of a thick, blunt airfoil at moderate Reynolds numbers ($3.1 \times 10^5 < Re_c < 7.25 \times 10^5$) using synthetic jet fluidic control near the airfoil leading edge. Preliminary results of this investigation were previously reported by Smith et al.[15] and Amitay et al.[16] Of particular interest are the effects of the jet placement, the momentum coefficient, and the control effectiveness at frequencies that are well above the natural shedding frequency of the airfoil.

## II. Experimental Setup

The airfoil model comprises an aerodynamic fairing, based on the aft portion of a NACA four-digit series symmetric airfoil, attached to a circular cylinder. The fairing section was fabricated out of a rigid foam material with an epoxy–fiberglass overlay. The surfaces of the cylinder and of the fairing are well polished. The cylinder is machined from an aluminum tube, and the fairing is fabricated using a special lamination and molding. The transition between the surface of the cylinder and the edge of the fairing is designed to have a close fit, and the surface discontinuity at the edge of the overlap domain is less than 0.1 mm. This surface discontinuity is not sufficient to trigger flow separation. In fact, based on the present pressure measurements (to be presented) the separation point at low angles of attack is downstream of the junction and at the large angles of attack moves upstream of the junction. The gap between the cylinder and fairing is specifically designed to prevent leakage between the pressure and suction sides of the airfoil, and at a given angle of attack and actuator jet angle, the junction between the cylinder and the fairing is sealed with thin (less than 0.05 mm) tape. The thickness of the assembled airfoil is 6.22 cm, and the combined cylinder–fairing chord is 25.4 cm, that is, $t/c = 0.24$ (Fig. 1). The cylinder is instrumented with 47 pressure taps that are located in the spanwise midplane and are equally spaced circumferentially around the cylinder. Similarly, the fairing is instrumented with 45 pressure taps along the top and bottom surfaces and at the same spanwise location as the taps on the cylinder. The pressure data are obtained using two 48-channel Scanivalve systems, and a 10-torr Baratron pressure transducer is used to obtain mean pressure data. The resolution of the pressure transducer is 0.001% of full scale of 10 torr.

The airfoil is mounted in an open-return, low-speed wind tunnel having a square test section measuring 91 cm on a side. The maximum air speed is $32 \pm 1$ m/s with a freestream turbulence level less than 0.25%. The upper and lower walls of the wind tunnel are adjusted to compensate for blockage created by the airfoil. For the airfoil, wall interference effects are estimated to result in a 1.5–2% overprediction of the drag coefficient.

The control jet is synthesized from two, side-by-side, 0.5-mm-wide, rectangular synthetic jet actuators that are parallel along their long spanwise dimension and are 2.5 mm apart in the freestream direction. The jet actuators span the center 140 mm of the cylinder, and they can be positioned at an azimuthal angle $\gamma$ between $-90$ to $+90$ (at $\alpha = 0$ deg) relative to the incoming flow direction by rotating the cylinder independently of the fairing. Two fences are placed at the edges of the actuator orifice to maintain a nominally two-dimensional flow in the controlled section of the airfoil. The fences are two cylinder diameters in height.

The actuator performance is measured using the momentum coefficient $C_\mu$,

$$C_\mu = \bar{I}_j \Big/ \tfrac{1}{2}\rho_0 U_0^2 c \tag{1}$$

where $\bar{I}_j$ is the time-averaged jet momentum per unit length during the outstroke, $\rho_0$ is the freestream fluid density, $c$ is the chord, and $U_0$ is the freestream velocity. The averaged momentum during the blowing cycle of the jet is

$$\bar{I}_j = \frac{1}{\tau}\rho_j b \int_0^\tau u_j^2(t)\,\mathrm{d}t \tag{2}$$

where $\tau = T/2$, $T$ is the period of the diaphragm motion,[13] $\rho_j$ is the jet density, $b$ is the jet orifice width, and $u_j(t)$ is the phase-averaged velocity at the jet exit plane. In the present work, $C_\mu$ is varied between $10^{-6}$ and $10^{-3}$.

Each of the two side-by-side synthetic jet actuators is driven with four piezoceramic disks. As noted earlier, in the present work the actuation frequency is deliberately selected to be well above $F^+ > \mathcal{O}(10)$ and, thus, is uncoupled from the natural unstable frequency of the separating shear layer. The natural shedding frequency of the stalled airfoil in the present work is $F^+ \approx 0.7$, that is, $f \approx 50$ Hz, and so $F^+$ of $\mathcal{O}(10)$ is nominally 700 Hz. Whereas

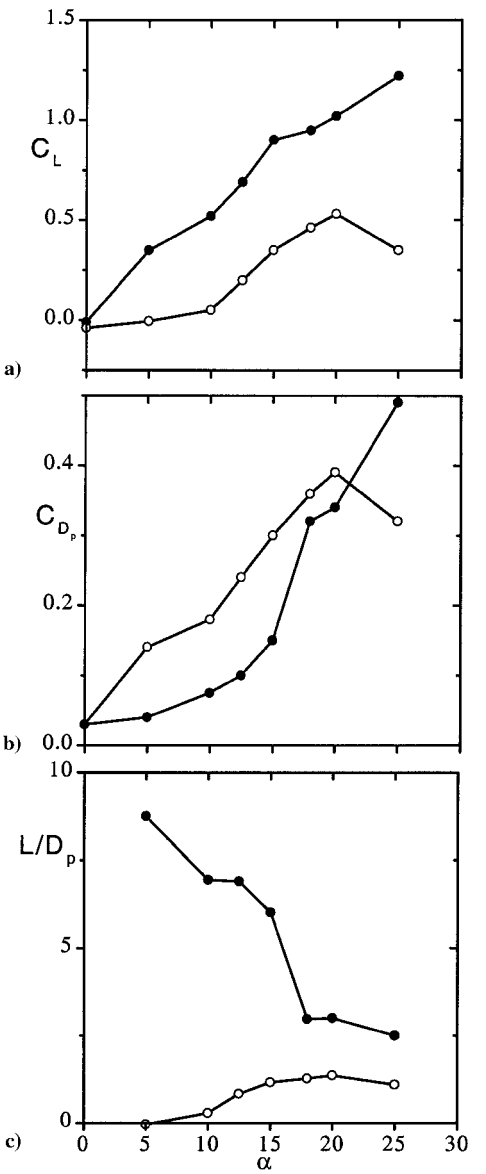


**Fig. 3 Forced (●) and unforced (○) cases: a) lift coefficient, b) pressure drag coefficient, and c) lift-to-pressure drag ratio vs angle of attack $\alpha$ for $\gamma = 60$ deg.**

the present actuator design has a relatively flat frequency response within the frequency band of interest, the jet momentum has a local maximum at 740 Hz, which was selected to be the operating frequency to maximize the range of $C_\mu$.

A second synthetic jet actuator is used to investigate the control effect at low actuation frequencies that are within the receptivity range of the separated shear layer. Similar to the setup of Williams et al.,[7] the jets are created by acoustically exciting the hollow cylinder section of the airfoil with two high pressure speakers (frequency response 60–5000 Hz) mounted on opposite ends of the cylinder. The low-frequency actuation utilizes the entire volume of the cylinder cavity, and the frequency response of the ensuing synthetic jets was measured (for a given input amplitude) using hot-wire anemometry. The resonance frequency of the jet cavity is approximately 110 Hz (corresponding to $F^+ = 1.5$), and the jet is calibrated (outside of the wind tunnel) at a given $C_\mu$ (up to $3.5 \times 10^{-3}$) over a broad frequency range [up to $F^+ \sim \mathcal{O}(10)$].

## III. Results and Discussion

Distributions of the pressure coefficient around the circumference of the airfoil for the forced (closed symbols) and unforced (open symbols) cases are shown in Figs. 2a–2f for six angles of attack: 0, 5, 10, 15, 20, and 25 deg, respectively. The error in the angle is ±0.5 deg. The chord Reynolds number is $Re_c = 3.1 \times 10^5$, and the angle of the jets (relative to the oncoming freestream) is $\gamma = 60$ deg. The momentum coefficient is $C_\mu = 3.5 \times 10^{-3}$.

At $\alpha = 0$ deg (Fig. 2a), the unforced flow is attached over the entire airfoil surface. These data show that although the suction peak is almost the same on both sides of the airfoil there are slight differences in the region where the fairing meets the cylinder. It appears that despite the asymmetry of the actuation, the pressure distributions on the top and bottom become more similar with control. At higher angles of attack, $\alpha \geq 5$ deg, the airfoil stalls without control. For $\alpha \leq 15$ deg (Figs. 2b–2d), the flow becomes fully reattached when control is applied, and the resulting pressure distributions exhibit a large suction peak near $x/c = 0.1$, which is in the vicinity of the point of maximum thickness. A rapid pressure recovery occurs for $0.1 < x/c < 0.2$, and thereafter the pressure recovery toward the trailing edge is gradual. Note that at $\alpha = 5$ and 10 deg in the absence of actuation (Figs. 2b and 2c, respectively), the pressure on the upper surface of the airfoil is actually higher than on the lower surface ($0.075 < x/c < 0.30$ for $\alpha = 5$ deg and $0.06 < x/c < 0.22$ for $\alpha = 10$ deg) and consequently, the overall lift force is reduced. However, when the jets are activated, the flow becomes fully attached, and the pressure on the upper surface is continuously lower through $x/c = 0.62$ and 0.72 ($\alpha = 5$ and 10 deg, respectively) where the pressure difference between the two surfaces is reversed through the trailing edge. This indicates that the streamwise rate of pressure recovery resulting from reattached flow on the upper surface exceeds the rate of recovery associated with the curvature of the bottom surface (relative to the oncoming flow). This effect decreases with increasing angle of attack where the pressure distribution on the lower surface becomes almost invariant with $x/c$ (Figs. 2d and 2e) and finally decreases with $x/c$ (Fig. 2f).

At $\alpha = 20$ deg (Fig. 2e), the control produces only partial reattachment. The flow remains attached through $x/c = 0.22$, but subsequently separates and, therefore, the pressure distribution is almost identical to the distribution in the absence of control. When $\alpha = 25$ deg (Fig. 2f), the unforced flow separates farther upstream, $x/c = 0.02$, resulting in a higher pressure within the separated flow region and less overall lift. Although the suction peak of the forced flow is lower for $\alpha = 25$ deg than it is for 20 deg, separation still occurs at the same streamwise location, $x/c = 0.2$. As a result, the pressure in the separated region of the forced flow is actually lower than for the unforced flow. Whereas the increase in the pressure difference (compared to the unforced flow) results in increased lift, at these angles of attack there is also a significant increase in pressure drag. Nevertheless, as shown in Fig. 3, the lift-to-pressure drag ratio increases compared to the unforced case.

The pressure distribution on the airfoil is integrated to yield the lift coefficient, the pressure drag coefficient, and the lift-to-pressure drag ratio over a range of angles of attack (Figs. 3a–3c, respectively).

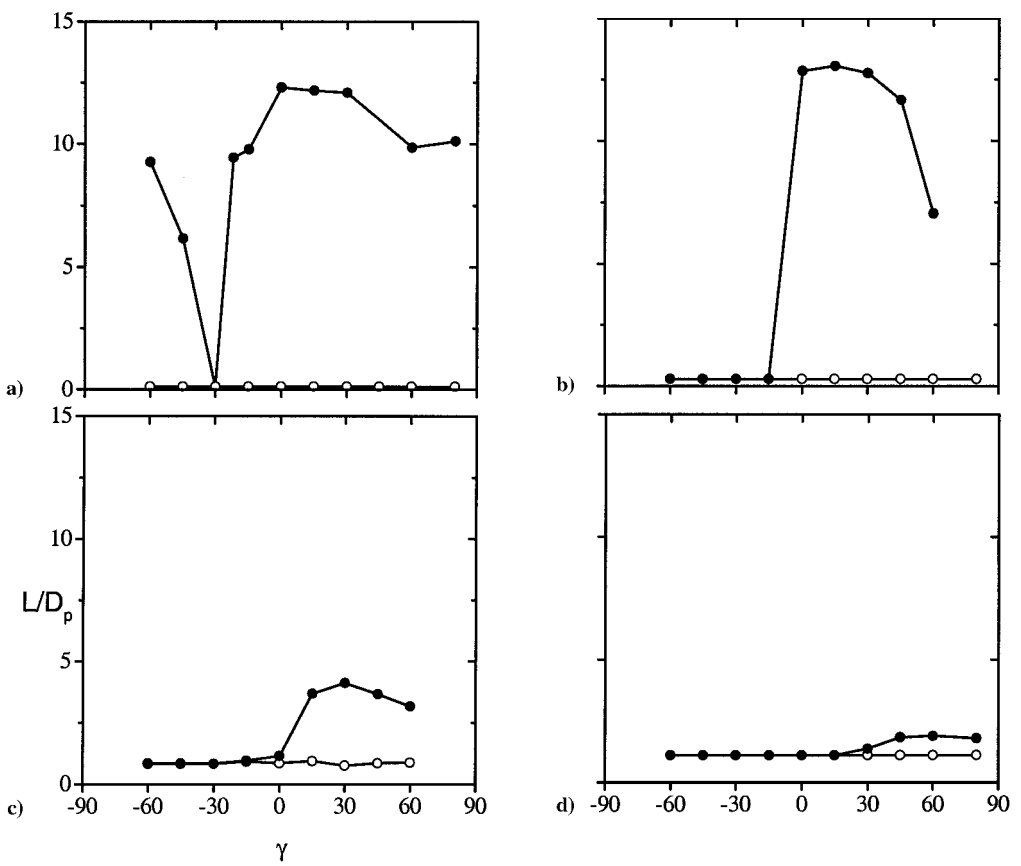


**Fig. 4 Forced (●) and unforced (○) cases; lift-to-pressure drag ratio vs the jets' location $\gamma$: a) $\alpha = 5$ deg, b) $\alpha = 10$ deg, c) $\alpha = 15$ deg, and d) $\alpha = 25$ deg.**

The corresponding distributions of the unforced flow are also shown for comparison (open symbols). Clearly, without control, the aerodynamic performance of this airfoil is poor (e.g., the lift-to-pressure drag ratio at $\alpha = 5$ deg is 0.115), and the airfoil is stalled even at small angles of attack. However, with actuation ($\gamma = 60$ deg, $C_\mu = 3.5 \times 10^{-3}$), the lift coefficient increases almost linearly with angle of attack as might be expected for a conventional thin airfoil. Furthermore, in the controlled cases, reattachment of the flow on the airfoil results in a reduced pressure drag coefficient. For example at $\alpha = 5$ deg, the pressure drag decreases by 45% with respect to the unforced case. Even at relatively high angles of attack, $\alpha = 25$ deg, where the flow is only partially reattached, the lift curve has yet to exhibit the downturn characteristic of stall. However, the monotonically increasing pressure drag (which exceeds the drag coefficient on the unforced airfoil at $\alpha = 25$ deg) and the pressure distribution (Fig. 2f) suggest that stall is imminent. Figure 3c shows that control significantly improves the lift-to-pressure drag ratio through the entire range of angles of attack. At $\alpha = 5$ deg, this ratio is increased by almost two orders of magnitude. However, as the angle of attack increases, the improvement in the $L/D_p$ diminishes.

In the results reported so far, the control jets are located upstream of the separation point. However, the work of Amitay et al.[1,2] showed that the control jets can be effective when placed both upstream and downstream of the nominal separation point of a circular cylinder. In what follows, the effect of jet location and $C_\mu$ on flow control is investigated over the same range of angles of attack as shown in Figs. 2 and 3.

Figures 4a–4d show the variation of the lift-to-pressure drag ratio with the jet angle $\gamma$ (relative to the incoming flow) for $\alpha = 5$, 10, 15, and 25 deg, respectively for the forced (closed symbols) and unforced (open symbols) flows at $C_\mu = 3.5 \times 10^{-3}$. As shown in Fig. 3c, the low lift-to-pressure drag ratio, $L/D_p = 0.115$, in the absence of control at $\alpha = 5$ deg is substantially improved when the jets are located at $\gamma = 60$ deg. However, Fig. 4a shows that at $\alpha = 5$ deg the optimal location of the jets is at $\gamma = 0$ deg, where $L/D_p$ increases from 0.115 to 12.2. Note that, at this angle of attack, $L/D_p$ increases substantially when the azimuthal location of the jets extends to $-60$ deg, which is on the pressure side of the airfoil. This behavior is not observed at larger angles of attack. Note also that at $\gamma = -30$ deg, the control effectiveness decreases sharply before recovering at $\gamma = -45$ deg (this apparent anomaly will be further discussed subsequently). Finally, it is remarkable that the reattachment of the separated flow can occur when the control is placed on the pressure side of the airfoil.

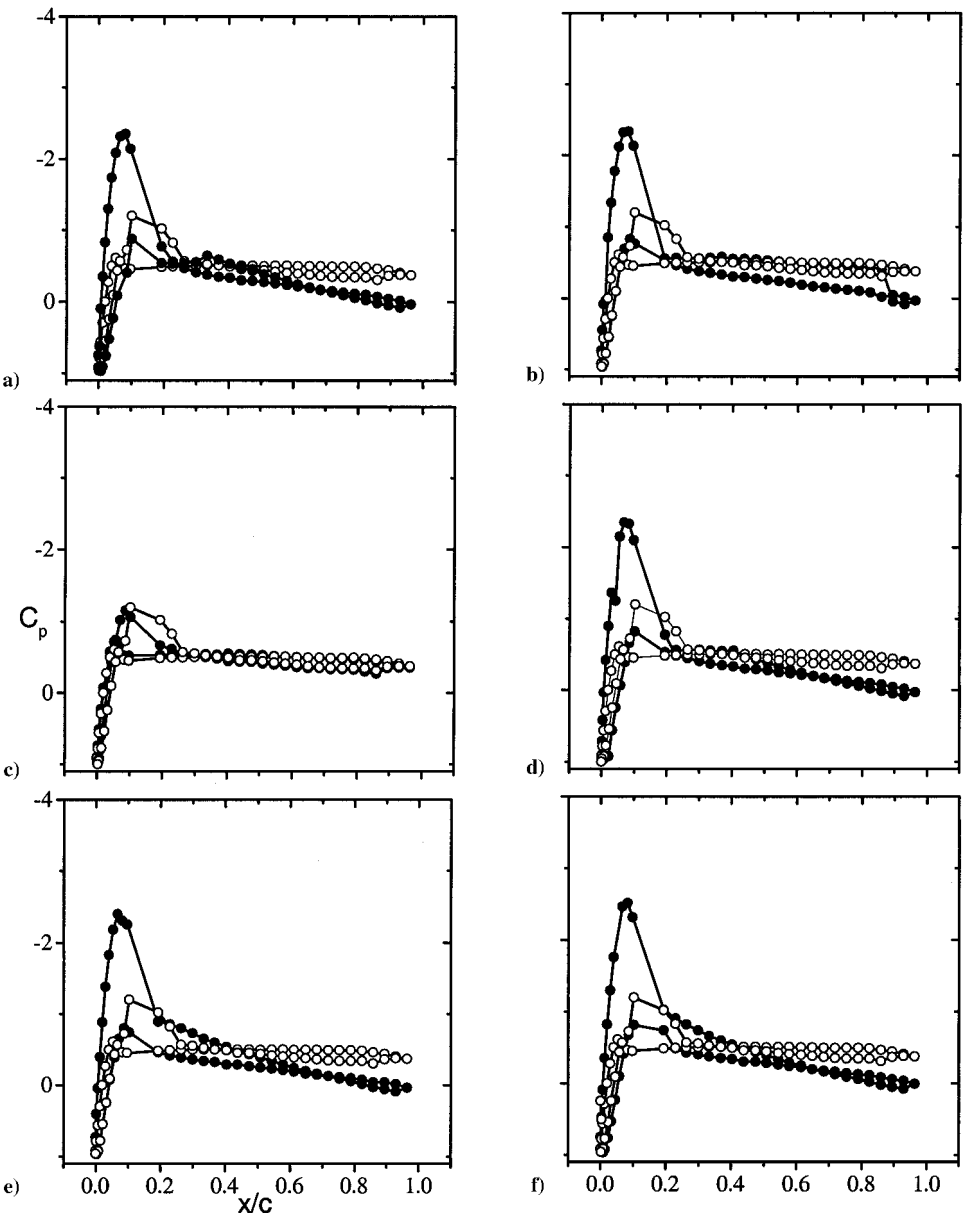


**Fig. 5 Forced (●) and unforced (○) cases; pressure coefficient distributions around the airfoil at different angles of the actuation jets: a) $\gamma = -60$ deg, b) $\gamma = -45$ deg, c) $\gamma = -30$ deg, d) $\gamma = -22$ deg, e) $\gamma = 0$ deg, and f) $\gamma = 60$ deg.**

As $\alpha$ increases, $L/D_p$ remains unchanged for negative $\gamma$, but then increases with $\gamma$ at threshold values that increase with angle of attack (Figs. 4b–4d). That is, as $\alpha$ increases and the separation point on the uncontrolled airfoil moves upstream, the most effective location of actuation (for fixed $C_\mu$) moves aft toward the separation point. Note also that a modest degree of proportional control in the $L/D_p$ can be obtained by varying $\gamma$.

The changes in the pressure distributions at $\alpha = 5$ deg for different $\gamma$ are shown in Figs. 5a–5e. The variation in $L/D_p$ with $\gamma$ that is apparent in Fig. 4a is revealed in the pressure distributions (on the suction side) as a separation bubble (manifested by a region of constant $C_p$) that varies in size with $\gamma$. When $\gamma$ is varied along the pressure side of the leading edge, a degree of proportional control over the size of this separation bubble can be achieved. With control applied on the pressure surface, $\gamma = -60$ deg (Fig. 5a), a closed separation bubble lying between $0.2 < x/c < 0.3$ on the lifting surface is apparent, and the stagnation point moves down along the lower surface. Rotating the control jets around the leading edge and more in alignment with the incoming flow near the stagnation point, $\gamma = -45$ deg (Fig. 5b) reduces the control effectiveness and increases the size of the separation bubble. For this value of $\gamma$, the separation bubble extends to $x/c = 0.9$. There is a narrow range of $\gamma$ near $-30$ deg where the control has only a minor effect (Fig. 5c). Yet interestingly, control applied at a location closer to the stagnation point, $\gamma = -22$ deg, does cause reattachment (Fig. 5d). Note that at this latter location, $\gamma = -22$ deg, the jets are approximately collocated with the mean stagnation point location (detailed discussion follows). Finally, for this angle of attack, $\alpha = 5$ deg, and level of control input, $C_\mu = 3.5 \times 10^{-3}$, actuation at $\gamma \geq 0$ deg (Figs. 5e and 5f) works equally well irrespective of the jet location and, within the resolution of the pressure measurements, eliminates the separation bubble altogether.

To show more clearly the location of the jets relative to the incoming flow direction, detailed plots of the pressure distributions at $\alpha = 5$ deg near the front stagnation point are shown in Figs. 6a–6d. Here, $C_p$ is plotted as a function of the cylinder azimuthal coordinate $\theta$, and the arrows indicate the location of the control jets. At the stagnation point, $C_p = 1$, and the pressure and suction sides are on its left and right, respectively. Observe that for the unforced case, the front stagnation point is at $\theta_{sp} \approx -5$ deg ($x/c|_{sp} \approx 0.002$); whereas, for the forced cases, the stagnation point moves to the lower surface with $x/c|_{sp}$ values between 0 and 0.007 ($\theta_{sp} \approx -20$ deg). Despite the detailed pressure measurements, a viable physical mechanism that explains this localized reduction in control effectiveness remains elusive. Some insight may be gained from velocity field measurements, for example, using particle image velocimetry, taken phase locked to the actuation waveform. The observations at these values of $\gamma$ suggest that the control is effecting a global change in the flow field. As suggested by earlier synthetic jet work[1,2] and demonstrated in the recent work of Honohan et al.,[17] the interaction between the control jets and the oncoming flow leads to localized mean displacement of the oncoming flow and, as a result, to modification of the streamwise pressure gradients. It may be argued that control effects may be understood in terms of the effect of nose drop in mitigating separation on the lifting surface of an airfoil. Finally, for angles of attack greater than 5 deg, the pressure distribution of the unforced flow is such that when the present actuation is applied on the pressure surface of the airfoil it has no observed effect on separation.

The sensitivity of the actuation effectiveness to jet location on the lifting surface suggests that the momentum coefficient $C_\mu$ may be in excess of the minimum required to effect control. Therefore, additional pressure measurements were made at fixed $\gamma$ and $\alpha$ while varying $C_\mu$. Figures 7a–7c show the lift coefficient, the pressure drag coefficient, and the lift-to-pressure drag ratio, respectively, as a function of $C_\mu$ for three different $\gamma$, 15, 45, and 60 deg, at $\alpha = 10$ deg. Despite some scatter in the data, Fig. 7 clearly shows the actuator performance level required to reattach the separated flow as a function of control location. Not unexpectedly, the closer the control is located to the observed separation point on the unforced airfoil, the less power is required to reattach the flow. A noteworthy observation is that actuation at $\gamma = 60$ deg ($x/c = 0.061$) requires two orders of magnitude less actuator performance than actuation at $\gamma = 15$ deg ($x/c = 0.004$). For $\alpha = 10$ deg, the optimum actuation location is at $\gamma = 45$ deg. However, when the jets are located at $\gamma = 15$ deg, they

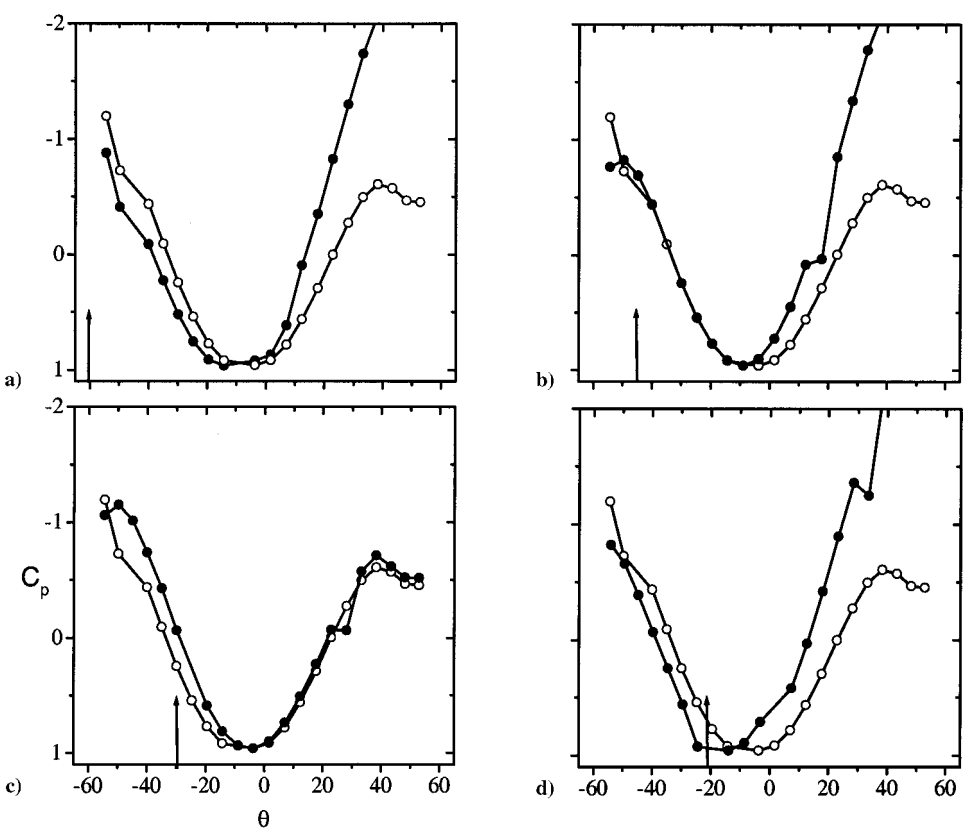


**Fig. 6 Pressure coefficient distributions near the front stagnation point as a function of the cylinder azimuthal coordinate $\theta$ at different angles of the actuation jets; forced (●) and unforced (○): a) $\gamma = -60$ deg, b) $\gamma = -45$ deg, c) $\gamma = -30$ deg, and d) $\gamma = -22$ deg.**

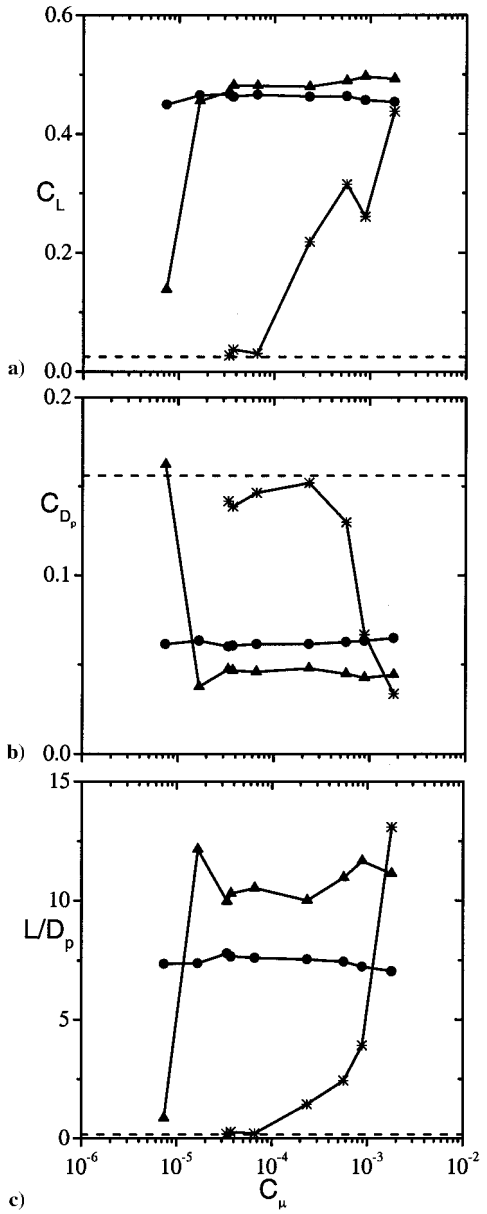


**Fig. 7 a) Lift coefficient, b) pressure drag coefficient, and c) lift-to-pressure drag ratio vs momentum coefficient $C_\mu$ for $\alpha = 10$ deg; ✳, $\gamma = 15$ deg; ▲, $\gamma = 45$ deg; and ●, $\gamma = 60$ deg. Dashed lines represent the unforced values.**

enable proportional control of the separated flow with momentum coefficient. Moreover, although at $\gamma = 60$ and even 45 deg $L/D_p$ appears to begin to decrease at higher levels of $C_\mu$, it continues to increase at $\gamma = 15$ deg. This suggests that even though relatively high levels of $C_\mu$ are necessary to affect the flow far enough upstream of separation, the interaction of the jets with the crossflow is more robust and can yield higher level of $L/D_p$ that may not be realizable when the jets are closer to the point of separation.

Figures 8a–8c and 8d–8f show detailed changes in the distributions of the pressure coefficient as $C_\mu$ increases for $\alpha = 10$ deg and $\gamma = 15$ and 45 deg, respectively. Similar to the proportional control with $\gamma$ at $\alpha = 5$ deg (Fig. 6), the proportional control of the separated flow with $C_\mu$ at $\gamma = 15$ deg is distinguished by the formation of a separation bubble on the lifting surface that decreases in size with increasing $C_\mu$. At $C_\mu = 1.1 \times 10^{-3}$ (Fig. 8a), a separation bubble of significant extent appears on the upper surface of the airfoil. (When $C_\mu$ is decreased to values less than $2.5 \times 10^{-4}$, the effect of the jets is insignificant.) As $C_\mu$ increases to $1.56 \times 10^{-3}$ (Fig. 8b), the flow becomes attached to the upper surface, although the suction peak near the leading edge is virtually unchanged. At the highest $C_\mu$ attained in the present experiments, $C_\mu = 3.5 \times 10^{-3}$ (Fig. 8c), the flow becomes completely attached to the upper surface and develops a significant suction peak.

For $\gamma = 45$ deg (Figs. 8d–8f), the range of $C_\mu$ for proportional control is too narrow to be resolved in the present experiments, and the control either attaches the flow completely to the upper surface or has no effect at all. For $C_\mu = 1.28 \times 10^{-5}$ (Fig. 8d), there are minute differences between the unforced and forced flows. However, as $C_\mu$ is roughly doubled, $C_\mu = 2.85 \times 10^{-5}$ (Fig. 8e), a strong suction peak appears on the upper surface, and the pressure distribution remains nearly unchanged when $C_\mu$ is increased to $4.13 \times 10^{-4}$ (Fig. 8f). Note that when $\gamma = 15$ deg, an increase in $C_\mu$ results in a subtle increase in the pressure distribution on the pressure side of the airfoil downstream of the front stagnation point (Fig. 8c). This increase, which is not effected when $\gamma = 45$ deg even for higher levels of $C_\mu$, contributes to both an increase in lift and a reduction in drag. It is conjectured that these effects are connected with the apparent change in the shape of the airfoil when the jets are placed at $\gamma = 15$ deg.

Figure 9 shows the dependence of the lift-to-pressure drag ratio on $C_\mu$ at three chord Reynolds numbers, $Re_c = 3.1 \times 10^5$, $5.25 \times 10^5$, and $7.25 \times 10^5$, for $\alpha = 15$ deg and $\gamma = 60$ deg. The actuation frequency is increased with $U_0$ to maintain $F^+ = 10$. In the absence of control, $L/D_p$ is approximately constant ($L/D_p = 0.82 \pm 0.02$ is marked with a dashed line) for all three Reynolds numbers. With control, $L/D_p$ increases to a nominal value of 3.6 and, at least within the present range of measurements, is independent of the Reynolds number and $C_\mu$ (except for $C_\mu > 10^{-3}$ at $Re_c = 3.1 \times 10^5$). The invariance of $L/D_p$ with Reynolds number and $C_\mu$ is not unexpected, and in fact similar trends were reported by Seifert et al.[18] for chord Reynolds numbers ranging from $10^5$ to $10^7$. However, note that in the present experiments $F^+ \sim \mathcal{O}(10)$, whereas in the experiments of Seifert et al.[18] $F^+$ was less than 2.

Although in the present work the aerodynamic forces are all time averaged, unsteady effects may be surmised by considering power spectra of the streamwise velocity in the wake of the airfoil. A hot-wire probe is placed in the wake of the airfoil, one chord length downstream of the trailing edge and on the lower side of the wake at a cross-stream elevation where the streamwise velocity deficit is one-half the maximum deficit (Fig. 10). The (dimensionless) frequency content of the hot-wire signal $\nu^+ = (f \cdot c)/U_0$ is examined in the presence and absence of actuation. The velocity spectrum of the unforced flow (dashed line) includes a strong spectral peak at the (natural) shedding frequency, $\nu^+ = 0.7$, and begins to decay at higher frequencies, $\nu^+ > 1.4$. With control (solid line), the turbulent kinetic energy throughout the entire spectrum is significantly reduced, and there is no discernible peak that corresponds to the passage frequency of organized vortical structures. It is remarkable that high-frequency actuation leads not only to the appearance of a featureless spectrum (and consequently, a steady reattachment) but also to the emergence of a spectral band having a $-\frac{5}{3}$ slope indicating enhanced dissipation.

As noted in Sec. I, much of the work on the active delay of flow separation has focused on extending the flight envelope of conventional airfoils using time-periodic actuation having a characteristic period that is comparable to the characteristic timescale, that is, time of flight, of the flow over the controlled surface. When the ratio between the characteristic time of flight and the actuation period, that is, the dimensionless frequency $F^+$, is of order one, the actuation frequency is also comparable to the shedding frequency of the body. In the present and earlier[1,2] work, the actuation frequency is deliberately selected to be at least an order of magnitude above the natural (or shedding) frequency of the airfoil, to broaden the bandwidth of the actuation and to enable coupling to flow features within the boundary layer upstream of separation. Thus, the effect of actuation frequency on the controllability of the separated flow is a paramount issue in the application of synthetic jets to flow control. Some details of the interaction between a synthetic jet and a crossflow are discussed in detail in the recent work of Honohan et al.[17]

To demonstrate the effect of the actuation frequency on the control effectiveness, the actuators are activated at six frequencies corresponding to $F^+ = 0.95$, 2.05, 3.4, 10, 14.7, and 20 (71, 148, 246, 740, 1088, and 1480 Hz, respectively). At $F^+ = 0.95$, 2.05, and 3.4,

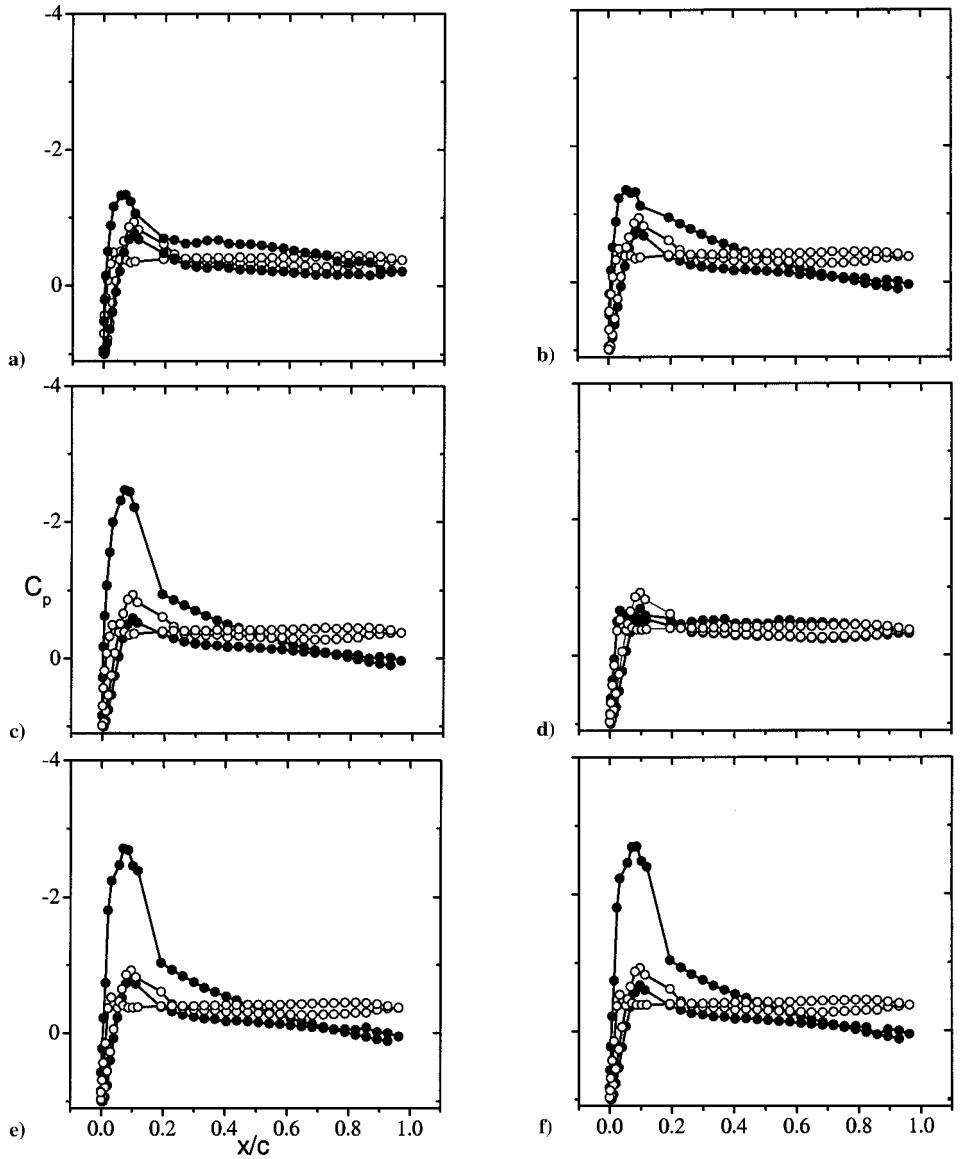


**Fig. 8 Forced (●) and unforced (○) cases, pressure coefficient distributions around the airfoil at different jets' locations, $\gamma$, and momentum coefficients $C_\mu$: a) $\gamma = 15$ deg, $C_\mu = 4.75 \times 10^{-4}$, b) $\gamma = 15$ deg, $C_\mu = 7.42 \times 10^{-4}$, c) $\gamma = 15$ deg, $C_\mu = 1.5 \times 10^{-3}$, d) $\gamma = 45$ deg, $C_\mu = 6.2 \times 10^{-6}$, e) $\gamma = 45$ deg, $C_\mu = 1.3 \times 10^{-5}$, and f) $\gamma = 45$ deg, $C_\mu = 1.9 \times 10^{-4}$.**

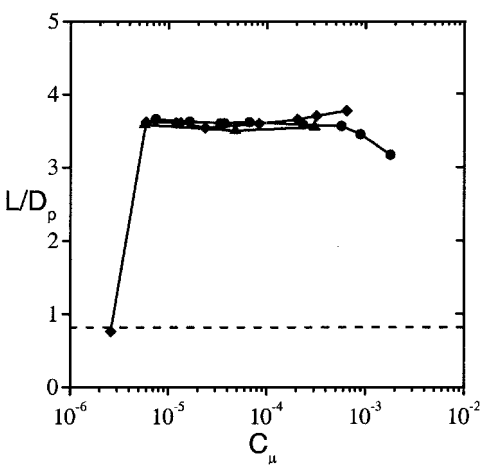


**Fig. 9 Lift-to-pressure drag ratio as a function of the momentum coefficient $C_\mu$ for ●, $Re_c = 3.1 \times 10^5$; ♦, $Re_c = 5.25 \times 10^5$; and ▲, $Re_c = 7.25 \times 10^5$.**

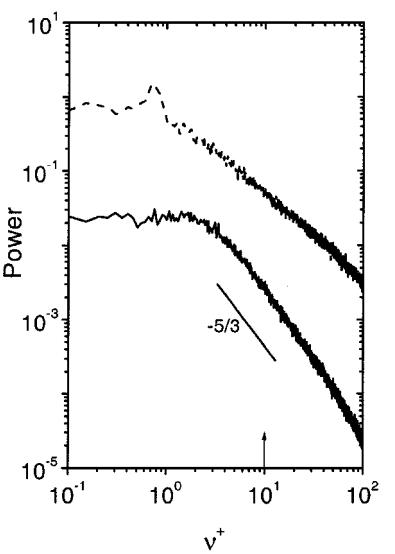


**Fig. 10 Unforced (· · · ·) and forced (——) at $F^+ = 10$ power spectra measured at $x/c = 2$, at $\alpha = 17.5$ deg and $\gamma = 60$ deg.**

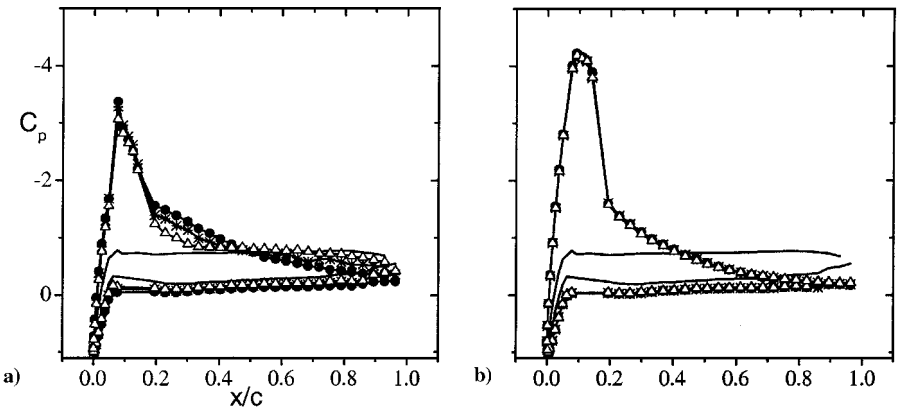


**Fig. 11 Pressure coefficient distributions around the airfoil at different dimensionless frequencies $F^+$: a) $F^+ = 0.95$ (●), 2.05 (✳), and 3.4 (△) and b) $F^+ = 10$ (●), 14.7 (✳), and 20 (∧).**

the jets are driven by audio speakers, whereas at high frequencies the jets are formed by compact actuators using piezoceramic disk drivers (cf. Sec. II). As noted in Sec. II, the actuators are calibrated at each operating frequency outside of the wind tunnel and then once again in the presence of a crossflow in the wind tunnel. It is found that when the operating frequencies are below $F^+ < 4$ the jets driven by the speaker actuators are spanwise uniform (along the long dimension of the orifice). However, at higher frequencies, the speaker-driven jets develop spanwise nonuniformities due to three-dimensional acoustic effects within the actuator cavity. Velocity measurements (not shown here) within the actuator orifice using a miniature hot-wire sensor reveal that for $F^+ > 4$ the performance of the speaker-driven actuator jets is markedly different in the presence and absence of a crossflow. In fact, in the presence of a crossflow, the velocity of the speaker-driven jets diminishes by more than 80%, and thus, their ability to reattach the flow is reduced. In contrast, the piezoelectric actuator, with a small cavity tuned to a high frequency, has a uniform output at the orifice that leads to a complete reattachment of the separated flow.

Distributions of the pressure coefficient around the airfoil for $F^+ = 0.95$, 2.05, and 3.4 and $F^+ = 10$, 14.7, and 20 are shown in Figs. 11a and 11b, respectively (the shedding frequency of the unforced flow is $F^+ = 0.7$). The pressure distribution for the unforced stalled flow (solid line) is also shown for reference. Actuation at low frequencies (Fig. 11a) results in a very sharp suction peak near $x/c = 0.075$, which corresponds to the location of the separation in the unforced flow. Concomitantly, the degree of pressure recovery toward the trailing edge is reduced with increasing control frequency, leading to an increase in pressure drag. The pressure distributions for $F^+ = 10$ (Fig. 11b), which is over an order of magnitude higher than the shedding frequency ($F^+ = 0.7$), are significantly different and exhibit larger and wider suction peaks with a corresponding larger increase in the lift coefficient. Following the suction peak, the pressure difference between the suction and pressure sides is smaller than at corresponding stations at the low actuation frequencies resulting in a lower pressure drag. Moreover, whereas at low actuation frequencies (Fig. 11a) the pressure distribution varies with $F^+$, at high actuation frequencies (Fig. 11b) the pressure distribution appears to be independent of $F^+$, suggesting that, when the actuation frequency is high enough, the details of the flow reattachment become independent of the frequency.

Detailed pressure distributions near the leading edge of the airfoil, $x/c < 0.1$, are shown in Fig. 12. These data emphasize that the effect of the actuation at both frequencies is measurable about the entire airfoil and that the increase in circulation in the forced flow results in a slight displacement of the front stagnation point toward the pressure side of the airfoil. Although the spatial resolution of the data is limited, these (and other data) suggest that low-frequency actuation introduces mean blockage upstream of the jets that is manifested by a reduction in the magnitude of the (negative) streamwise pressure gradient. Downstream of the jets, the static pressure decreases further before pressure recovery begins at $x/c > 0.12$. For the high

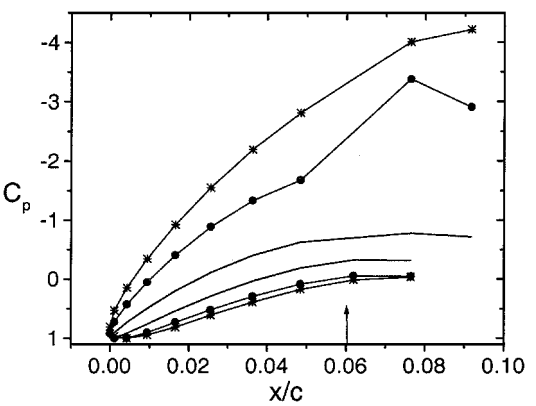


**Fig. 12 Detailed pressure coefficient distributions near the leading edge of the airfoil, $x/c < 0.1$; unforced (——), $F^+ = 1.1$ (●), and $F^+ = 10$ (✳).**

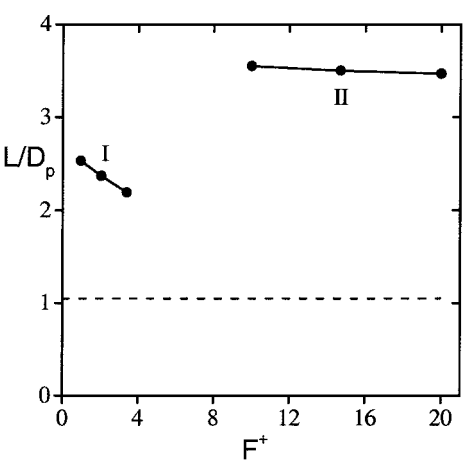


**Fig. 13 Variation of the lift-to-pressure drag ratio with dimensionless actuation frequency $F^+$ for $\gamma = 60$ deg with the unforced value shown as dashed line.**

actuation frequency jet, $F^+ = 10$, the details of the changes in the pressure distribution upstream and downstream of the control jets are apparently not resolved by the present pressure measurements but were derived from the measurements of Honohan et al.[17]

The variation of the lift-to-pressure drag ratio with actuation frequency is shown in Fig. 13. Two distinct domains are immediately apparent. In the first domain (I), where the actuation frequencies are of the same order as the shedding frequency, $F^+ < 4$, the $L/D_p$ decreases with increasing $F^+$ (from 2.65 for $F^+ = 0.95$ to 2.35 for $F^+ = 3.3$, which might be expected from stability considerations of the separated shear layer). In the second domain (II in Fig. 13), the actuation frequency is more than an order of magnitude higher

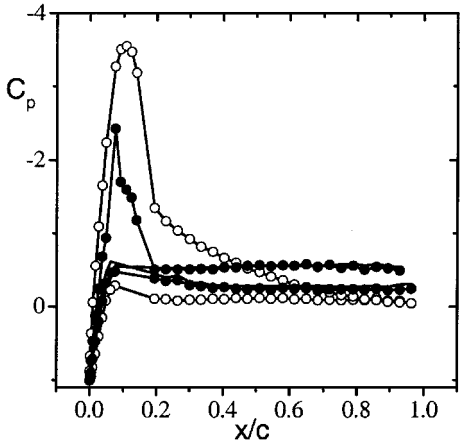


**Fig. 14 Pressure coefficient distributions around the airfoil at $F^+ = 10$ using ●, audio speakers; ○, piezoelectric drivers; and ——, unforced flow.**

than the shedding frequency, $F^+ \geq 10$, and the lift-to-pressure drag is higher, $L/D_p = 3.2$, and appears to be independent of the actuation frequency, suggesting that the mechanism that leads to the suppression of separation is not associated with the stability of the separated shear layer. Note that bandwidth limitations of the low- and high-frequency actuators prevented overlap within the domain $4 < F^+ < 10$.

Finally, Fig. 14 compares the pressure distribution for the airfoil with an audio-speaker actuator operating at $F^+ = 10$ to the pressure distribution for the airfoil with the piezoelectric actuator operating at $F^+ = 10$. For additional comparison, the unforced (solid line) and forced distributions are coplotted. Here, the airfoil is at $\alpha = 15$ deg, control is applied at $\gamma = 60$ deg, nominal $C_\mu = 3.5 \times 10^{-3}$, and the chord Reynolds number is $Re_c = 3.1 \times 10^5$. From Fig. 14, it is clear that at high actuation frequencies, the effectiveness of the synthetic jet actuators is greatly influenced by the design of the cavity and the driver.

## IV. Conclusions

The reattachment of separated flow on an unconventional symmetric airfoil using synthetic jet actuators is investigated. The cylinder model of Amitay et al.[1,2] is modified to give a 24% thick airfoil section with cylindrical leading edge. Mean surface static pressure measurements are used to elucidate the time-averaged effects of the actuation on the separated flow. In the absence of control, the airfoil stalls for $\alpha \geq 5$ deg; however, with control, fully attached flow can be achieved for $\alpha \leq 17.5$ deg, and partial reattachment with some recovery of lift is achieved up to the maximum angle tested, $\alpha = 25$ deg. The present work has shown that both the location and the strength of the control input affect the extent of the reattached flow. Dramatic increases in lift (up to 100%) and decreases in pressure drag (up to 45%) are observed as a result of flow reattachment, although for $\alpha > 17.5$ deg, the increase in lift is accompanied by an increase in drag. Control is effective up to a chord Reynolds number of $7.25 \times 10^5$, and the data suggest that for a given $C_\mu$ and jet angle $\gamma$ the lift-to-pressure drag ratio is independent of the Reynolds number.

From a design point of view, these measurements reveal that if either the separation location is unknown or practical limitations preclude control near separation the location of the control $\gamma$ or the momentum coefficient $C_\mu$ may be manipulated to obtain the best performance of the airfoil for the entire range of angles of attack.

The effect of the actuation frequency is also considered. The synthetic jets are operated over a range of frequencies up to a dimensionless frequency $F^+ = 20$, which is about 30 times higher than the natural shedding frequency of the separated flow over the airfoil. Two distinct performance regimes are observed. When the actuation frequency is of the same order as the shedding frequency of the stalled airfoil, $F^+ < 4$, an increase in the actuation frequency leads to a reduction in the recovered lift-to-pressure drag ratio. When the actuation frequency is more than an order of magnitude larger than the shedding frequency, $F^+ \geq 10$, the lift-to pressure drag ratio is much larger and appears to be invariant with the actuation frequency. The present work has also shown that the performance of actuators with large cavities is degraded when these actuators are driven at high frequencies. This performance degradation is due, in part, to three-dimensional acoustic effects inside of the cavity and velocity nonuniformities along the actuator orifice.

Future work will focus on the dynamics of controlled flow reattachment and separation effected by synthetic jet actuators and the role of the actuation frequency in these processes.

## Acknowledgments

This work was supported by Air Force Office of Scientific Research Grant F49620-96-1-0194 (monitored by T. Beutner, M. Glauser, and J. M. McMichael), and McDonnell Douglas Aerospace (now The Boeing Company, St. Louis). The authors would also like to acknowledge a number of useful discussions with J. Donovan, L. Kral, and R. Wlezien.

## References

[1]Amitay, M., Honohan, A., Trautman, M., and Glezer, A., "Modification of the Aerodynamic Characteristics of Bluff Bodies Using Fluidic Actuators," AIAA Paper 97-2004, June 1997.

[2]Amitay, M., Smith, B. L., and Glezer, A., "Aerodynamic Flow Control Using Synthetic Jet Technology," AIAA Paper 98-0208, Jan. 1998.

[3]Ahuja, K. K., and Burrin, R. H., "Control of Flow Separation by Sound," AIAA Paper 84-2298, Jan. 1984.

[4]Zaman, K. B. M. Q., Bar-sever, A., and Mangalam, S. M., "Effect of Acoustic Excitation on the Flow over a Low-Re Airfoil," *Journal of Fluid Mechanics*, Vol. 182, 1987, pp. 127–148.

[5]Huang, L. S., Maestrello, L., and Bryant, T. D., "Separation Control over an Airfoil at High Angles of Attack by Sound Emanating from the Surface," AIAA Paper 87-1261, 1987.

[6]Hsiao, F.-B., Liu, C.-F., and Shyu, J.-Y., "Control of Wall-Separated Flow by Internal Acoustic Excitation," *AIAA Journal*, Vol. 28, No. 8, 1990, pp. 1440–1446.

[7]Williams, D., Acharya, M., Bernhardt, J., and Yang, P., "The Mechanism of Flow Control on a Cylinder with the Unsteady Bleed Technique," AIAA Paper 91-0039, Jan. 1991.

[8]Chang, R.-C., Hsiao, F.-B., and Shyu, R.-N., "Forcing Level Effects of Internal Acoustic Excitation on the Improvement of Airfoil Performance," *Journal of Aircraft*, Vol. 29, No. 5, 1992, pp. 823–829.

[9]Hsiao, F.-G., Shyu, R.-N., and Chang, R.-C., "High Angle-of-Attack Airfoil Performance Improvement by Internal Acoustic Excitation," *AIAA Journal*, Vol. 32, No. 3, 1994, pp. 655–657.

[10]Seifert, A., Bachar, T., Koss, D., Shepshelovich, M., and Wygnanski, I., "Oscillatory Blowing: A Tool to Delay Boundary-Layer Separation," *AIAA Journal*, Vol. 31, No. 11, 1993, pp. 2052–2060.

[11]Seifert, A., Darabi, A., and Wygnanski, I., "Delay of Airfoil Stall by Periodic Excitation," *Journal of Aircraft*, Vol. 33, No. 4, 1996, pp. 691–698.

[12]Donovan, J. F., Kral, L. D., and Cary, A. W., "Active Flow Control Applied to an Airfoil," AIAA Paper 98-0210, Jan. 1998.

[13]Smith, B. L., and Glezer, A., "The Formation and Evolution of Synthetic Jets," *Physics of Fluids*, Vol. 10, No. 9, 1998, pp. 2281–2297.

[14]Smith, B. L., and Glezer, A., "Vectoring and Small-Scale Motions Effected in Free Shear Flows Using Synthetic Jet Actuators," AIAA Paper 97-0213, Jan. 1997.

[15]Smith, D. R., Amitay, M., Kibens, V., Parekh, D. E., and Glezer, A., "Modification of Lifting Body Aerodynamics Using Synthetic Jet Actuators," AIAA Paper 98-0209, Jan. 1998.

[16]Amitay, M., Kibens, V., Parekh, D. E., and Glezer, A., "Flow Reattachment Dynamics over a Thick Airfoil Controlled by Synthetic Jet Actuators," AIAA Paper 99-1001, Jan. 1999.

[17]Honohan, A. M., Amitay, M., and Glezer, A., "Aerodynamic Control Using Synthetic Jets," AIAA Paper 2000-2401, June 2000.

[18]Seifert, A., and Pack, L. G., "Oscillatory Control of Separation at High Reynolds Numbers," AIAA Paper 98-0214, Jan. 1998.

M. Samimy
*Associate Editor*